A Flocking-Based Paradigm for Hierarchical Cyber-Physical Smart Grid Modeling and Control

Jin Wei, *Student Member, IEEE,* Deepa Kundur, *Senior Member, IEEE,* Takis Zourntos, *Senior Member, IEEE,* and Karen L. Butler-Purry, *Senior Member, IEEE*

***Abstract*—It is well known that information will play an important role in enhancing emerging smart grid system operation. Therefore, questions naturally arise as to when the increased data-dependence may be considered excessive. Two practical considerations emerge: 1) communications and computational overhead, in which redundant and irrelevant information acquisition and use results in heavy computational burden with limited performance return; and 2) increasing risks of power system disruption due to information delay from communication congestion or cyber attack. One strategy to improve smart grid resilience is to determine the appropriate degree of dependence on cyber information to balance performance with overhead and risk. In this paper, we present a hierarchical cyber-physical multiagent model of smart grid system operation based on flocking theory in the context of the transient stability problem. Through this model, we study strategies that harness a selective degree of cyber technology by leveraging physical couplings. Our formulation enables the identification of large-scale distributed control strategies for robust and resilient power grid operation. We demonstrate the potential performance improvements of our findings on the New England 39-bus power system for case studies involving a variety of system faults and communication delays.**

***Index Terms*—Cyber-physical modeling of smart grid, flocking-based dynamical systems, power system transient stability.**

I. Introduction

THE EFFECTIVE modeling of a power grid can significantly improve the understanding of its operation and design. In this paper, we consider a dynamical systems-based cyber-physical representation that aims to provide power system designers with insights on how to leverage distributed control to maintain transient stability in the face of significant disruptions. Recent work has just begun to address this problem. Ilić *et al.* [1] propose a dynamic framework to represent the interactions amongst generators and loads. Here a module with linear closed-loop dynamics is used to represent each generator and load that are interconnected using a linear network model of the system. Li and Han [2] study how the addition of communication links can effectively restabilize a faulted power grid. They employ a linearized swing equation-based model relating the overall generator synchronization to spectral properties of a matrix that is a weighted sum of the Laplacian of the (physical) power graph and the (cyber) communication network. A greedy search algorithm is proposed to identify a communication topology that can enable synchronism for a given smart grid topology. Existing research by Wei. *et al.* [3] has studied the analogy between the dynamics of generator synchronization and that of flocking theory. A distributed cyber-physical control approach is developed such that in the face of disturbances, the system is restabilized by "steering" its dynamics as a cohesive flock.

Given the value of this flocking metaphor, in this paper we extend our work and make the following contributions. First, we formally explore how information and physical couplings can be synergistically harnessed for restabilizing a power grid under severe fault and cyber attack. Through analysis we assess how hierarchy and the selective use of cyber information can benefit scalability and robustness to information delay. Second, through a flocking-based paradigm we develop distributed control methodologies that leverage cooperation between external energy storage (EES) and traditional synchronous machines to maintain transient stability in the face of severe disturbances. Third, we introduce and apply the notion of state-dependent hierarchy in which coherent generator clusters from disturbance are leveraged such that strong physical couplings are identified to selectively apply distributed cyber-control where necessary. An algorithm to identify coherent clusters is presented. Simulations are conducted on New England 39-bus test system to demonstrate performance gains of our approach empirically.

II. Proposed Multiagent Framework

A. Cyber-Physical Integration

We model the cyber-physical integration in the smart grid with a two-tier hierarchical multiagent framework shown in Fig. 1. Each agent consists of the following functions.

1) A dynamic node representing a physical power system element, in this case a generator.

Manuscript received July 10, 2013; revised January 19, 2014, March 17, 2014, and May 28, 2014; accepted July 11, 2014. Date of publication August 8, 2014; date of current version October 17, 2014. This work was supported in part by the U.S. National Science Foundation under Grant ECCS-1028246, in part by the Norman Hackerman Advanced Research Program under Project 000512-0111-2009, and in part by the Natural Sciences and Engineering Research Council of Canada. Paper no. TSG-00516-2013.

J. Wei is with the Department of Electrical and Computer Engineering, University of Akron, Akron, OH 44325 USA (e-mail: jwei@uakron.edu).

D. Kundur is with the Department of Electrical and Computer Engineering, University of Toronto, Toronto, ON M5S 2E4, Canada (e-mail: dkundur@comm.utoronto.ca).

T. Zourntos is with the Ontario College of Art and Design University, Toronto, ON M5T 1W1, Canada (e-mail: tz12ji@student.ocadu.ca).

K. L. Butler-Purry is with the Department of Electrical and Computer Engineering, Texas A&M University, College Station, TX 77843 USA (e-mail: klbutler@tamu.edu).

Color versions of one or more of the figures in this paper are available online at http://ieeexplore.ieee.org.

Digital Object Identifier 10.1109/TSG.2014.2341211

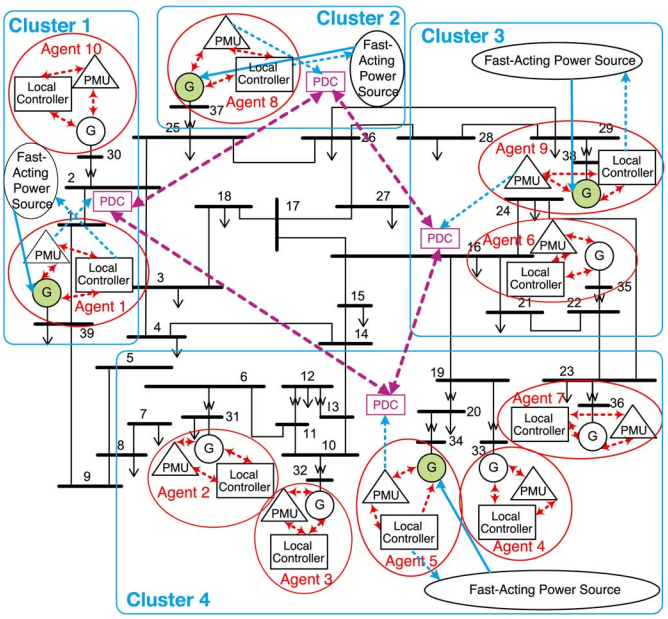

Fig. 1. Hierarchical cyber-physical control for New England 39-bus system.

2) A phasor measurement unit (PMU) that acquires generator phase angle and frequency data from the dynamic node.
3) A local cyber-controller that computes a control signal that is applied to the agent's generator using PMU data.

Each agent's frequency, phase angle, and coherency characteristics are those of its generator. The PMU and local controller are both considered to be cyber elements due to their data acquisition, communication and computation tasks.

The physical coherency between active agents is achieved by using our real-time dynamic coherency identification scheme. The agents with high physical coherency are considered to form a cluster and one agent within the cluster (typically with highest generator inertia) is selected as the lead agent. Only the lead agent's PMU and local cyber-control are activated for overall cluster regulation and the phasor data concentrator (PDC) in each cluster is implemented to guarantee synchronization of the data information flows amongst lead agents. Therefore, this enables a state-dependent system hierarchy whereby intercluster interactions are cyber-physical (tier-1) and intracluster synergies are physical (tier-2). Since our focus is on maintaining transient stability in the face of cyber-physical disturbance through distributed control that employs EES, each cluster also includes fast-acting energy storage(s), which in practice may include battery storage devices and flywheels.

B. Transient Stability

Power system transient stability describes the ability of a smart grid to remain in synchronism when subjected to large disturbances, such as transmission line faults and generator loss [4]. For smart grids, achieving transient stability consists of maintaining both exponential frequency synchronization and phase angle cohesiveness of its synchronous generators through application of distributed control.

Exponential frequency synchronization requires the frequencies of all the generators agree asymptotically with a common value f_0 typically set to 60 Hz and normalized in this formulation to 1. Letting ω_i be the normalized relative frequency of Generator i with respective to f_0, we can describe exponential frequency synchronization as follows:

$$\omega_i(t) \to 0, \ as \ \ t \to \infty. \tag{1}$$

As stated in [5], the loss of synchronism of generators results if the rotor angle difference between two generators is beyond a certain limit, which causes a rapid drop in bus voltages. Therefore, as shown in (2), phase angle cohesiveness necessitates that the difference between phase angles of Generators i and j should be below a predefined threshold γ

$$\left|\theta_i - \theta_j\right| \leq \gamma \tag{2}$$

where γ is normally set to $5\pi/9$ as discussed in [6]. The reader should note that other formulations [7], [8] have set the upper bound as $\pi/2$. The discrepancy is due to the fact that in our model, we consider transfer conductances and thus are able to relax the upper bound from 90° to 100° as supported in [5] and [6].

C. Flocking

Flocking is a behavior exhibited by groups of birds participating in a shared objective such as flying to a mutual destination. Such behavior enables a collective to accomplish an objective difficult to achieve individually through a combination of cooperation, consensus and informed-adaptation. Members of a flock are referred to as flockmates or agents. The behavior within a flock has been described by a following set of heuristic agent-interaction rules that we employ [9].

1) *Flock Centering:* Agents attempt to stay close to nearby flockmates.
2) *Collision Avoidance:* Agents avoid collisions with nearby flockmates.
3) *Velocity Matching:* Agents attempt to match velocity with nearby flockmates.

Based on these three rules, Olfati-Saber [10] provided a framework for design and analysis of scalable distributed flocking algorithms using a double integrator model: $\dot{\mathbf{q}} = \mathbf{p}$ and $\dot{\mathbf{p}} = \mathbf{u}$, where $\mathbf{q} \in \mathbb{R}^N$ is the position vector of the flockmates, $\mathbf{p} \in \mathbb{R}^N$ denotes the velocity vector, $\mathbf{u} \in \mathbb{R}^N$ represents the control signal, and N is the size of the flock. To achieve the flocking objectives $\mathbf{u}$ is comprised of three terms, $\mathbf{u} = -\nabla V(\mathbf{q}) - \mathbf{L} \cdot \mathbf{p} + F\left(\mathbf{p}, \mathbf{q}, \mathbf{p}_r, \mathbf{q}_r\right)$, where the first term is the gradient of a potential energy function $V(\mathbf{q})$ that characterizes system objectives and constraints. The second represents a velocity consensus protocol where $\mathbf{L}$ is the Laplacian matrix associated with the flock communication graph. Finally, the third models navigational feedback designed to ensure each agent tracks a reference $(\mathbf{p}_r, \mathbf{q}_r)$.

By studying the three flocking rules, we notice that flock centering and the velocity matching are analogous to the phase angle cohesiveness and the exponential frequency synchronization objectives in the transient stability problem, respectively. This inspires us to reformulate the problem of transient stability as a task of flocking formation control.

D. Dynamics and Interaction

Assuming there are N agents in general, each is assigned a coupled dynamical system equation to model the cyber-physical interactions. To describe the physical system, we make use of the well-known interconnected swing equations to describe rotor dynamics [4] of the Kron-reduced [11] power system as detailed in [7] and [8] to give the following dynamical representation for each agent:

$$M_i\dot{\omega}_i = -D_i\omega_i + P_{m,i} - |E_i|^2 G_{ii} - \sum_{j=1,j\neq i}^{N} P_{ij}\sin\left(\theta_i - \theta_j + \varphi_{ij}\right) \tag{3}$$

where $i \in \{1, 2, \ldots, N\}$ represents the generator index, θ_i denotes the rotor phase angle measured with respect to a rotating frame reference at frequency $f_0 = 60$ Hz, $\omega_i = \dot{\theta}_i$ is the normalized relative frequency, $M_i > 0$ and $D_i > 0$ represent the generator inertia and the damping parameters, respectively, and E_i, $P_{m,i}$ and G_{ii} are the internal voltage, mechanical power input and equivalent shunt conductance of Generator i, respectively. $P_{ij} = |E_i||E_j||Y_{ij}|$ and $\varphi_{ij} = \arctan\left(G_{ij}/B_{ij}\right)$ where Y_{ij}, G_{ij} and B_{ij} are the Kron-reduced equivalent admittance, conductance and susceptance, respectively, between Generators i and j. It should be noted that we explicitly include the transfer conductances in our model reflected in φ_{ij} to avoid oversimplification.

In our framework, the cyber network (PMU data + local controllers) is integrated into this framework through controlling the fast-acting EES power absorption/injection, $P_{u,i}$, to Generator Bus i to compensate for fluctuations in demand power in the system after a severe disturbance. We define the control signal $u_i = P_{u,i}$ (for $t > t_0$) to have initial condition $u_i = 0$ p.u. for $t \leq t_0$, where t_0 is the time at which the local controllers initiate the control commands. Letting α_i be a binary number defined as follows:

$$\alpha_i = \begin{cases} 1, \text{ if the } i\text{th agent is the lead agent} \\ 0, \text{ otherwise} \end{cases} \tag{4}$$

we can formulate the dynamics of our cyber-physical integrated framework as follows:

$$M_i\dot{\omega}_i = -D_i\omega_i + P_{m,i} - E_i^2 G_{ii} - \sum_{j=1,j\neq i}^{N} \underbrace{P_{ij}}_{\text{phys §}} \sin\left(\theta_i - \theta_j + \underbrace{\varphi_{ij}}_{\text{phys §}}\right) + \underbrace{\alpha_i u_i}_{\text{cyber §}} \tag{5}$$

where physical interagent couplings (denoted phys §) are characterized by parameters P_{ij} and φ_{ij} and cyber couplings (cyber §) through u_i. For normal operation $u_i = 0$. However, when a disturbance strikes, u_i will excite the system to reachieve (transient) stability.

III. Proposed Two-Tier Hierarchical Cyber-Physical Control Protocol

We design the control signal u_i under two assumptions. First, we assume that, in the face of severe disturbance, $u_i = P_{u,i}$ changes much faster than the mechanical power input $P_{m,i}$ for each agent and the time span to recover transient stability is short; thus we treat $P_{m,i}$ as a constant during the procedure of maintaining transient stability. This assumption is reasonable for future smart grids where fast-response energy storage such as battery storage and flywheels will be available to inject and absorb energy for periods of brief control. Second, we assume that the problems of voltage regulation and frequency synchronization are decoupled. This enables us to consider the voltage E_i as a constant during controller excitation to reachieve the frequency synchronization.

In order to reformulate the problem of cyber-physical control for maintaining transient stability as a task of flocking formation control, as stated in Section II-C, we intend to present the dynamics of each agent in our cyber-physical integrated system, which is originally formulated in (5), in the form of a double integrator model. Under the two assumptions stated above, computing derivatives of the both sides of (5), and reformulating gives

$$\begin{cases} \dot{\boldsymbol{\theta}} = \boldsymbol{\omega} \\ \mathbf{D}\dot{\boldsymbol{\omega}} = -\mathbf{M}\ddot{\boldsymbol{\omega}} - \mathbf{L}\boldsymbol{\omega} + \boldsymbol{\alpha}\dot{\mathbf{u}} \end{cases} \tag{6}$$

where the index assignments are reordered such that Agents $i = 1, \ldots, C$ correspond to lead agents, C is the number of clusters in our hierarchical framework, $\boldsymbol{\alpha} = \mathbf{diag}\,[\alpha_1, \ldots, \alpha_N]$, $\alpha_i = 1$ for $i \leq C$, and $\alpha_i = 0$ otherwise. $\boldsymbol{\theta} = [\theta_1, \ldots, \theta_N]^T$, $\boldsymbol{\omega} = [\omega_1, \ldots, \omega_N]^T$, $\mathbf{u} = [u_1, \ldots, u_N]^T$, $\mathbf{M} = \mathrm{diag}\,[M_1, \ldots, M_N]$, $\mathbf{D} = \mathrm{diag}\,[D_1, \ldots, D_N]$, and $\mathbf{L}$ is a $N \times N$ physical coupling matrix whose elements can be represented as

$$l_{ij} = \begin{cases} \sum_{j=1,j\neq i}^{N} P_{ij}\cos\left(\theta_i - \theta_j + \varphi_{ij}\right), & \text{if } i = j \\ -P_{ij}\cos\left(\theta_i - \theta_j + \varphi_{ij}\right), & \text{if } i \neq j. \end{cases} \tag{7}$$

We define the control signal $\mathbf{u}$ as

$$\dot{\mathbf{u}} = \tilde{\mathbf{u}} + \mathbf{L}\boldsymbol{\omega} - \mathbf{B}\boldsymbol{\omega} \tag{8}$$

where $\tilde{\mathbf{u}}$ is a new control vector derived from $\mathbf{u}$ and $\mathbf{B}$ is a predesigned $N \times N$ cyber coupling diagonal matrix whose diagonal element $B_i \geq (100 \times D_i)$. Based on (8), we can rewrite (6) as follows:

$$\begin{cases} \dot{\boldsymbol{\theta}} = \boldsymbol{\omega} \\ (\mathbf{D} + \boldsymbol{\alpha}\mathbf{B})\,\dot{\boldsymbol{\omega}} = -\mathbf{M}\ddot{\boldsymbol{\omega}} + \boldsymbol{\alpha}\tilde{\mathbf{u}}. \end{cases} \tag{9}$$

In practice, for the ith synchronized generator, the ratio between the inertia M_i and the damping parameter D_i satisfies $M_i/D_i \in \mathcal{O}(10)$ [6]. We therefore find that the associated perturbation parameter for Lead Agent i, which has $\alpha_i = 1$ is $\epsilon_i = M_i/(D_i + B_i) \in \mathcal{O}(0.1)$ representing an overdamped system, which enables the application of singular perturbation techniques to in (9) to study the dynamics of the lead agents over a longer time scale. Specifically, applying singular perturbation analysis and letting $\mathcal{M}_i = D_i + B_i$ [12], where the index $i = 1, \ldots, C$, gives the form of a double integrator model as follows:

$$\begin{cases} \dot{\theta}_i = \omega_i \\ \mathcal{M}_i\dot{\omega}_i = \tilde{u}_i. \end{cases} \tag{10}$$

Here, the simplification has allowed the physical notion of generator "jerk" related to $\ddot{\omega}_i$, where $i = 1, \ldots, C$, to be eliminated from the dynamics.

A. Hierarchical Cyber-Physical Dynamics

In our hierarchical framework, the agents are grouped into the same cluster if they have high physical coherency, and we assert that the deviations between the states (i.e., phase angle and normalized relative frequency) of the secondary agents and their lead agents are very small. Therefore, we propose to treat the states (θ_i, ω_i) of secondary agent i as "noisy" versions of those of Lead Agent k which is in its cluster and estimate (θ_i, ω_i) as follows:

$$\begin{cases} \widehat{\omega}_i = \omega_k + \triangle_i \\ \widehat{\theta}_i = \theta_k + \varepsilon_i^0 + \varsigma_i \end{cases} \tag{11}$$

where ε_i^0 denotes the phase angle difference between the ith and kth agents in the static (prefault) state, and $\triangle_i \sim \mathcal{U}(-a, a)$ and $\varsigma_i \sim \mathcal{U}(-b, b)$ are uniform random noises on $[-a, a]$ and $[-b, b]$, respectively, with $a \ll 1$ and $b \ll 1$.

By using (11), we are able to estimate the information of the physical coupling matrix $\mathbf{L}$ by only using the lead agents' states. To simplify, we partition $\mathbf{L}$ as follows:

$$\mathbf{L} = \begin{bmatrix} \mathbf{R}_{C\times C} & \mathbf{S}_{C\times(N-C)} \\ \mathbf{T}_{(N-C)\times C} & \mathbf{U}_{C\times C} \end{bmatrix}.$$

By using (11), we can approximate the matrix $\mathbf{S}$ with $\widehat{\mathbf{S}}$ whose element is shown as follows:

$$\widehat{\mathbf{S}}(j,k) = -P_{jk}\cos\left(\theta_j - \theta_k - \varepsilon_i^0 + \varphi_{jk}\right) \tag{12}$$

where the ith secondary agent belongs to the kth cluster. Using (12), we can approximate the matrix $\mathbf{R}$ by using $\widehat{\mathbf{R}}$ whose element is defined as follows:

$$\widehat{\mathbf{R}}(i,j) = \begin{cases} \mathbf{R}(i,j), & \text{if } i \neq j \\ -\sum_{j=1,j\neq i}^{C} \mathbf{R}(i,j) - \sum_{j=C+1}^{N} \widehat{\mathbf{S}}(i,j), & \text{otherwise.} \end{cases} \tag{13}$$

Based on (8) to (13), the control signal for the lead agents, $\mathbf{u}_l$, can be calculated as follows:

$$\dot{\mathbf{u}}_l = \tilde{\mathbf{u}}_l + \left(\widehat{\mathbf{R}} + \widehat{\mathbf{S}}\Psi\right)\boldsymbol{\omega}_l - \mathbf{B}_l\boldsymbol{\omega}_l \tag{14}$$

where $\mathbf{u}_l = [u_1, \ldots, u_C]^T$, $\tilde{\mathbf{u}}_l = \left[\tilde{u}_1, \ldots, \tilde{u}_C\right]^T$, $\boldsymbol{\omega}_l = [\omega_1, \ldots, \omega_C]^T$, and $\mathbf{B}_l = \text{diag}[B_1, \ldots, B_C]$.

Based on (8) to (14), we achieve the hierarchical cyber-physical dynamics as follows.

1) *The Lead Agents (Tier-1):*

$$\begin{cases} \dot{\boldsymbol{\theta}}_l = \boldsymbol{\omega}_l \\ \boldsymbol{\mathcal{M}}_l\dot{\boldsymbol{\omega}}_l = \tilde{\mathbf{u}}_l - \widehat{\mathbf{S}}\boldsymbol{\Delta} \end{cases} \tag{15}$$

where $\boldsymbol{\Delta} = \left[\triangle_{C+1}, \ldots, \triangle_N\right]^T$, $\widehat{\mathbf{S}}\boldsymbol{\Delta}$ can be treated as random noise according to (11) and (12), $\boldsymbol{\theta}_l = [\theta_1, \ldots, \theta_C]^T$, $\boldsymbol{\mathcal{M}}_l = \mathbf{D}_l + \mathbf{B}_l$, $\mathbf{D}_l = \text{diag}[D_1, \ldots, D_C]$, and

$$\Psi(i,j) = \begin{cases} 1, \text{ if the } (C+i)\text{th agent is in the } j\text{th cluster} \\ 0, \text{ otherwise.} \end{cases}$$

2) *The Secondary Agents (Tier-2):*

$$\begin{cases} \dot{\boldsymbol{\theta}}_s = \boldsymbol{\omega}_s \\ \mathbf{D}_s\dot{\boldsymbol{\omega}}_s = -\mathbf{L}_s\boldsymbol{\omega}_s - \mathbf{M}_s\ddot{\boldsymbol{\omega}}_s \end{cases} \tag{16}$$

where $\mathbf{L}_s$ denotes the physical coupling matrix for secondary agents, $\mathbf{M}_s = \text{diag}\left[M_{C+1}, \ldots, M_N\right]$ $\boldsymbol{\theta}_s = \left[\theta_{C+1}, \cdots, \theta_N\right]^T$, and $\boldsymbol{\omega}_s = \left[\omega_{C+1}, \cdots, \omega_N\right]^T$. Because the associated local controllers and ESSs are not activated for the secondary agents, their dynamics as described in (16) is equivalent to the dynamics represented in (3).

B. Design by Analogy to Flocking

In [3], we presented a flocking-inspired nonhierarchical distributed control framework. In this paper, we propose a two-tier hierarchical control paradigm that leverages the physical coherency between the agents by applying flocking-based control only to lead agents. Specifically, we show in the Appendix that given an accurate identification of generator coherency [13], the following control law guarantees transient stability:

$$\tilde{\mathbf{u}}_l = -\Phi - \widetilde{\mathbf{L}}\boldsymbol{\omega}_l - c_1\left(\boldsymbol{\omega}_l - \boldsymbol{\omega}^*\right) \tag{17}$$

where c_1 is a positive parameter for the linear navigational feedback, $\boldsymbol{\omega}^* = \mathbf{0}$ is the desired normalized generator frequency, $\Phi = \nabla V(\boldsymbol{\theta}_l)$ is the gradient of $V(\boldsymbol{\theta}_l)$ with respect to $\boldsymbol{\theta}$, $V(\boldsymbol{\theta}_l)$ represents the potential energy function to guarantee that the phase angle difference between each pair of lead agents is bounded, which is defined as follows:

$$V(\boldsymbol{\theta}_l) = \frac{1}{2}\sum_{i=1}^{C}\sum_{j=1,j\neq i}^{C}\chi\left(\theta_i - \theta_j\right) \tag{18}$$

where $\chi(\cdot)$ is a pairwise attractive potential defined as

$$\chi(z) = \begin{cases} 0, & \text{if } |z| \leq \frac{5\pi}{9} \\ c_2\left(z^2 - \frac{25\pi^2}{81}\right)^2, & \text{otherwise} \end{cases}$$

where c_2 is a positive parameter to control the penalty level induced. Therefore, the gradient Φ can be represented as follows:

$$\Phi(i) = \sum_{j=1,j\neq i}^{C}\phi\left(\theta_i - \theta_j\right) \tag{19}$$

$$\phi(z) = \begin{cases} 0, & \text{if } |z| \leq \frac{5\pi}{9} \\ 4c_2 z\left(z^2 - \frac{25\pi^2}{81}\right), & \text{otherwise.} \end{cases}$$

The matrix $\widetilde{\mathbf{L}}$ is another $C \times C$ cyber coupling matrix designed to achieve frequency consensus and its ijth element is set as

$$\widetilde{l}_{ij} = \begin{cases} c_3, & \text{if } i = j \\ -\frac{c_3}{C-1}, & \text{otherwise.} \end{cases} \tag{20}$$

Substituting (17) into (15) and letting $\boldsymbol{\omega}^* = \mathbf{0}$, the lead agent dynamics becomes

$$\begin{cases} \dot{\boldsymbol{\theta}}_l = \boldsymbol{\omega}_l, \\ \boldsymbol{\mathcal{M}}_l\dot{\boldsymbol{\omega}}_l = -\Phi - \widetilde{\mathbf{L}}\boldsymbol{\omega}_l - c_1\boldsymbol{\omega}_l - \widehat{\mathbf{S}}\boldsymbol{\Delta} \end{cases} \tag{21}$$

which represents a linear second-order differential equation with respect to $\boldsymbol{\omega}_l$.

Based on (14) and (17), we have the following:

$$\dot{\mathbf{u}}_l = -\Phi + \left(\widehat{\mathbf{R}} + \widehat{\mathbf{S}}\Psi\right)\boldsymbol{\omega}_l - \widetilde{\mathbf{L}}\boldsymbol{\omega}_l - c_1\boldsymbol{\omega}_l - \mathbf{B}_l\dot{\boldsymbol{\omega}}_l. \tag{22}$$

By integrating both sides of (22), we can formulate $\mathbf{u}$, which represents the power transmission $\mathbf{P}_u$ between the fast-reacting power source and the synchronized generators, as

$$\mathbf{u}_l = \begin{cases} \mathbf{0}, & \text{for } t \le t_0 \\ \int_{t_0}^{t} \dot{\mathbf{u}}_l d\tau = -\boldsymbol{\Gamma} + \boldsymbol{\eta} - \boldsymbol{\varrho}, & \text{for } t > t_0 \end{cases} \tag{23}$$

where the C-dimension column vectors $\boldsymbol{\Gamma} = \int_{t_0}^{t} \Phi d\tau$, $\boldsymbol{\eta} = \int_{t_0}^{t} \left(\widehat{\mathbf{R}} + \widehat{\mathbf{S}}\Psi\right) \boldsymbol{\omega}_l d\tau$, and $\boldsymbol{\varrho} = \int_{t_0}^{t} \left(\widetilde{\mathbf{L}}\boldsymbol{\omega}_l + c_1\boldsymbol{\omega}_l + \mathbf{B}_l\dot{\boldsymbol{\omega}}_l\right) d\tau$. Each element of $\boldsymbol{\Gamma}$ is represented as follows:

$$\boldsymbol{\Gamma}(\boldsymbol{i}) = \sum_{j=1, j\neq i}^{C} \left[\int_{t_0}^{t} \phi\left(\theta_i - \theta_j\right) \right] d\tau \tag{24}$$

and each element of $\boldsymbol{\eta}$ can be obtained by using (7) and (12) as follows:

$$\begin{aligned} \boldsymbol{\eta}(i) = & \sum_{j=1, j\neq i}^{C} P_{ij} \sin\left(\theta_{ij} + \varphi_{ij}\right) \\ & + \sum_{j=1, j\neq i}^{C} \sum_{k\in\mathcal{I}_j} P_{ik} \sin\left(\theta_{ij} - \varepsilon_k^0 + \varphi_{ik}\right) - \eta_i^0 \end{aligned} \tag{25}$$

where $\mathcal{I}_j$ denotes the index set of the secondary agents belonging to the jth cluster, $\omega_{ij} = \omega_i - \omega_j$, $\theta_{ij} = \theta_i - \theta_j$, and

$$\begin{aligned} \eta_i^0 = & \left[\sum_{j=1, j\neq i}^{C} P_{ij} \sin\left(\theta_{ij} + \varphi_{ij}\right) \right. \\ & \left. + \sum_{j=1, j\neq i}^{C} \sum_{k\in\mathcal{I}_j} P_{ik} \sin\left(\theta_{ij} - \varepsilon_k^0 + \varphi_{ik}\right) \right]_{t=t_0}. \end{aligned}$$

Since $\widetilde{\mathbf{L}}$, c_1, and $\mathbf{B}_l$ are all constants, we can calculate each element of $\boldsymbol{\varrho}$ by using (20) as follows:

$$\begin{aligned} \boldsymbol{\varrho}(i) = & (c_1 + c_3) \int_{t_0}^{t} \omega_i d\tau - \frac{c_3}{C-1} \sum_{j=1, j\neq i}^{C} \int_{t_0}^{t} \omega_j d\tau \\ & + B_i \int_{t_0}^{t} \dot{\omega}_i d\tau = (c_1 + c_3)\left(\theta_i - \theta_i^0\right) \\ & - \frac{c_3}{C-1} \sum_{j=1, j\neq i}^{C} \left(\theta_j - \theta_j^0\right) + B_i\left(\omega_i - \omega_i^0\right) \end{aligned} \tag{26}$$

where ω_i^0 and θ_i^0, respectively, denotes the value of the normalized relative frequency and the rotor phase angle of Agent i at time $t = t_0$, which are both available.

Based on (23)–(26), we can conclude that by using the information of ω_i and θ_i of each lead agent, which are both available, the value of $\mathbf{u}_l$ can be calculated.

IV. Timely Dynamic Agent Coherency Identification

In our previous paper [14], we propose a timely dynamic agent coherency identification scheme which requires very short observation window. Our scheme transforms the data of agents' state from the observation space to an information space whereby the agents' frequencies and phases characterize the movement and dynamics of boids within multiple flocks with different features. Boid i carries 3-D information describing the ith agent's status at time $t = k$ as

$$\begin{cases} \mathcal{I}_i^1(k) = \theta_i(k) \\ \mathcal{I}_i^2(k) = \omega_i(k) \\ \mathcal{I}_i^3(k) = \delta_i(k) \end{cases} \tag{27}$$

where $\mathcal{I}_i(k) = [\mathcal{I}_i^1(k)\ \mathcal{I}_i^2(k)\ \mathcal{I}_i^3(k)]^T$, $\theta_i(k)$ and $\omega_i(k)$ are the phase angle and the normalized frequency, respectively, of the ith generator at the time step $t = k$ that are obtained directly from PMU information, and $\delta_i(k)$ is the acceleration of the ith generator at the time step $t = k$ estimated from the current and historical values of $\omega_i(k)$.

The state of Boid i is described as follows:

$$\mathcal{S}_i(k) = [\mathbf{p}_i(k), \mathbf{v}_i(k)]^T \tag{28}$$

where $\mathbf{p}_i(k), \mathbf{v}_i(k) \in \mathbb{R}^{2\times 1}$ denote the boid's position and the velocity, respectively. Two boids are considered to be neighbors at time step $t = k$ if the distance between them is less than the predetermined threshold d_c. Therefore, we define the set of neighbors for the ith boid as follows: $\mathcal{N}_i(k) = \{\forall j \| \mathbf{p}_i(k) - \mathbf{p}_j(k) \| < d_c\}$.

We compute the informational (feature) similarity between neighboring Boids i and j as follows. For $j \in \mathcal{N}_i(k)$

$$\zeta_{ij}(k) = \left| \sum_{n=1}^{3} \alpha_n \times \left(\mathcal{I}_i^n(k) - \mathcal{I}_j^n(k)\right) \right| \tag{29}$$

where $\{\alpha_n\}$ is a scalar weight determining the impact of specific information on boid interaction. Given a threshold value $\zeta_{th}(k)$, if $\zeta_{ij}(k) \le \zeta_{th}(k)$ they are assumed to be in the same flock and hence are called flockmates. Otherwise, they are assumed to be in different flocks.

As illustrated in detail in [14], we model the dynamics of Boid i based on their feature similarity and flocking rules as

$$\begin{cases} \mathbf{v}_i(k+1) = \mathbf{v}_i(k) + \Delta t \sum_{l=1}^{3} w_l \mathbf{g}_{i,l}(k) \\ \mathbf{p}_i(k+1) = \mathbf{p}_i(k) + \Delta t \mathbf{v}_i(k) \end{cases} \tag{30}$$

where $\mathbf{g}_{i,1}, \mathbf{g}_{i,2}, \mathbf{g}_{i,3}$ represent the accelerations calculated based on the flocking rules flock centering, velocity matching, and obstacle avoidance, respectively, w_l denotes the weight representing the impact of the component $\mathbf{g}_{i,l}$, and Δt is the algorithm time step for coherence identification.

Based on dynamic model in (30), we can plot the boids' trajectories in the information space and achieve the multiple flocks constituted by the boids, which corresponds to the clusters constituted by the agents having high physical coherency in the observation space.

V. Case Studies

We demonstrate the performance of our flocking-based two-tier hierarchical control framework with dynamics in (15) and (16) collectively also described by (5) in achieving transient stability for two case studies on the New England 39 Bus system as shown in Fig. 2 and detailed in [15] consisting of $C = 10$ generators. MATLAB/Simulink is employed for simulations. In each case, we illustrate the efficiency of our

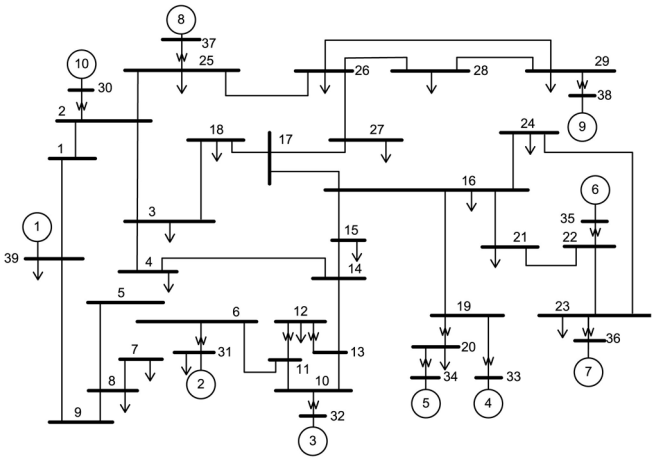

Fig. 2. New England 39-bus power system.

proposed hierarchical approach in selectively leveraging physical couplings to make use of cyber data and control selectively. In all (nonhierarchical and hierarchical) cases the cyber control parameters of (23) are set to $c_1 = 3$, $c_2 = 5$, and $c_3 = 1/10$, and the PMU sampling rate is 50 Hz. The power transmission limit for the fast-acting grid is set to $\mu = P_{u,i}/P_{r,i} \leq 1$ where $P_{r,i}$ is the rated power.

We compare our results to situations when no control is computed nor applied [corresponding to minimum information use and control and $\alpha_i = 0$ for all i in (5)] and when nonhierarchical control is applied [corresponding to maximum information use and control and $\alpha_i = 1$ for all i in (5)]. An efficient hierarchical framework would have comparable stabilizing performance to the latter case without the associated overhead. In each case, we also evaluate the performance of our hierarchical framework when experiencing cyber communication delay and practical constraints of fast-acting EES.

A. Ideal Environment

1) Case I: The system disturbance consists of a 3-phase short circuit in the middle of Line $14-15$ of Fig. 2 that occurs at time $t = 0$ s. The Line $14-15$ is removed at $t = 0.1$ s. Fig. 3 shows the normalized rotor frequencies and phase angles over a period of 10 s when no control is applied corresponding to (6) for $\alpha_i = 0$ for all i. Instability is clearly evident in all plots.

Fig. 4 (note: scale differs from Fig. 3) demonstrates the performance for nonhierarchical cyber-physical control activated at time $t = 0.15$ s, in which the PMU of each agent is activated and cyber control works at each agent corresponding to (6) for $\alpha_i = 1$ for all i. The EES power absorbtion/injection to each generator bus, determined by the control signal $\mathbf{u}_l$ of (23) is shown in Fig. 6. Even though the clipping of the control signal occurs due to the capacity limit previously discussed, transient stability is still achieved.

Our two-tier hierarchical cyber-physical control framework is implemented in three steps.

1) The proposed timely dynamic agent coherency identification scheme is implemented immediately after Line $14-15$ is removed at time $t = 0.1$ s. The corresponding boid trajectories introduced by our agent coherency identification scheme is presented in Fig. 8 for a brief observation period of $t = 0.05$ s; as described in (27), each boid carries the information describing the associated agent's status. The neighboring boids interact with each other based on the informational similarity which is defined in (29) and their dynamics are modeled in (30). From Fig. 8, we observe that agent coherency involves the following groups: $\{Agent_1\}$, $\{Agent_2, Agent_3\}$, and $\{Agent_4, \ldots, Agent_{10}\}$.

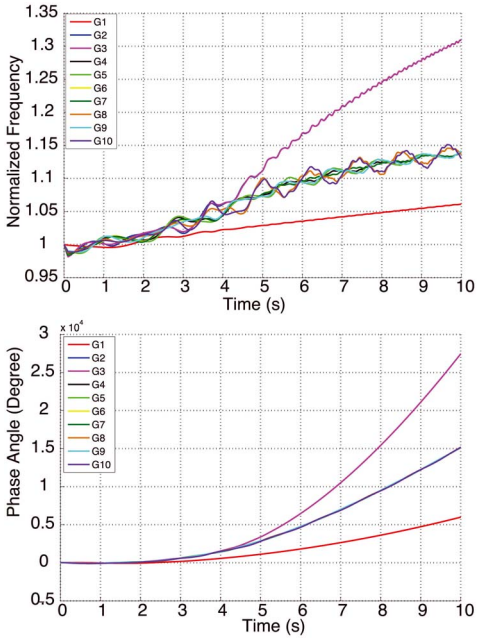

Fig. 3. Normalized rotor frequencies and phase angles without cyber control for Case Study I.

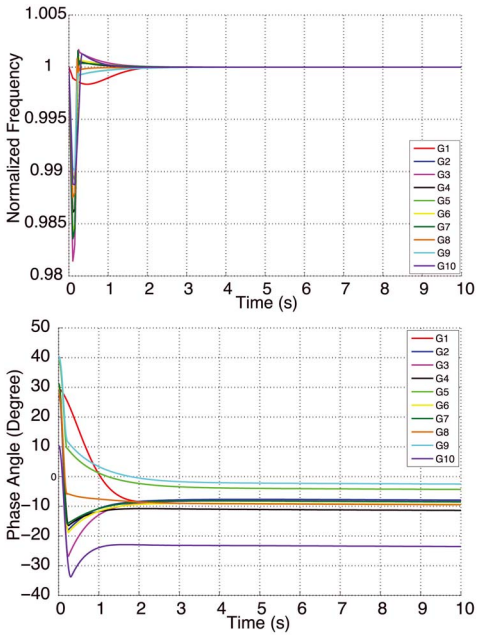

Fig. 4. Normalized rotor frequencies and phase angles with nonhierarchical control for Case Study I.

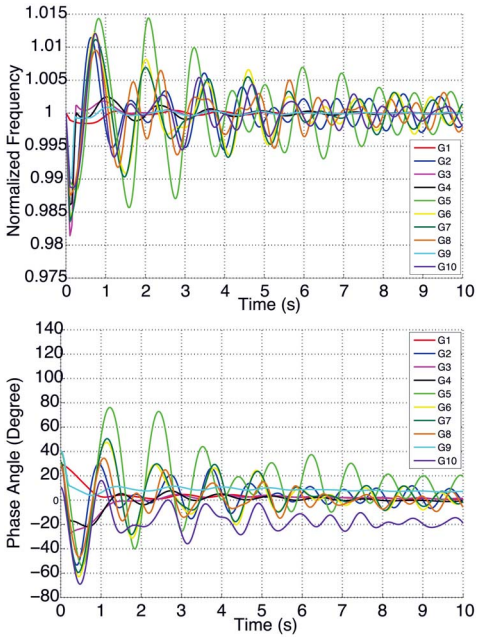

Fig. 5. Normalized rotor frequencies and phase angles with hierarchical control for Case Study I.

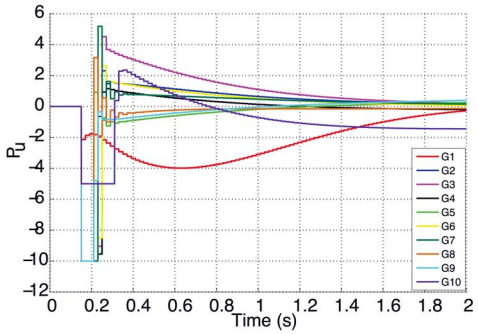

Fig. 6. Power transfer P_u by fast acting energy storage at generator buses in the presence of nonhierarchical control for Case Study I.

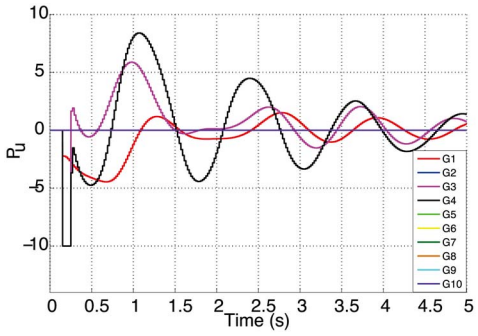

Fig. 7. Power transfer P_u by fast acting energy storage at generator buses in the presence of hierarchical control for Case Study I.

2) We then assign the groups as clusters and select the lead agents of the clusters as *Agent* 1, *Agent* 3, and *Agent* 4 given that they have the greatest inertia within their corresponding cluster.
3) At time $t = 0.15$ s, our proposed two-tier hierarchical control framework is activated which controls the fast-acting EES associated with each lead agent to absorb/inject power to the generator buses of the associated agents. Based on our proposed control framework, the power absorption/injection is calculated based on (23) and is plotted in Fig. 7. As shown in Fig. 7, the EESs of the Lead Agents 1, 3, 4 are activated to absorb power from the system at time $t = 0.15$ s and then adjust their power output at each time step $\Delta t = 20$ ms to track the command given by the associated local controllers. After time $t = 0.25$ s the power output of each EES sinusoidally decays to zero. In contrast to the EES power outputs for nonhierarchy, the sinusoidal oscillations are higher in frequency. This is because the hierarchical case represents an "under-actuated" version of the nonhierarchical such that the control applied to select generators must stabilize all of them. This requires that the associated control signals to be more "reactionary" and faster-moving.

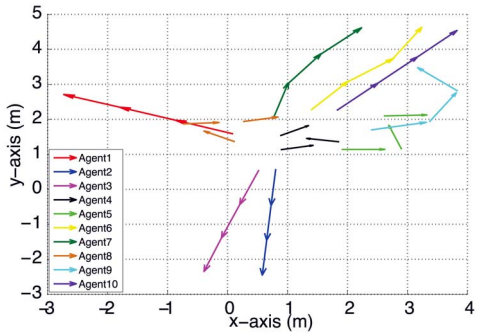

Fig. 8. Trajectories of the boids for Case Study I.

Fig. 5 presents the generator frequencies and phase angles when using hierarchical control. In contrast to Fig. 3, in which there is no control, transient stabilization is evident. In contrast to the nonhierarchical case shown in Fig. 4, there is more high frequency oscillatory behavior due to the nature of the activated EES power outputs. From Fig. 5, we deduce that although the information acquisition and control is selectively applied to lead agents only, the high physical coherency between the secondary agents and their associated agents ensures maintaining the transient stability of all the agents.

2) Case II: The system disturbance consists of a 3-phase short circuit occurs at time $t = 0$ s in the middle of Line $17 - 27$ of Fig. 2. The Line $17 - 27$ is removed at $t = 0.1$ s. Figs. 9 and 10 show the normalized rotor frequencies and phase angles over a period of 10 s when no control is applied. Based on Figs. 9 and 10, we assess transient stability of the system by calculating the power angle-based stability margin ξ [4], and achieve $\xi_1 = 57.1$ which implies that the system transient security is low and very sensitive to perturbation. Parameter $\xi = ((360 - \delta_{\max})/(360 + \delta_{\max})) \times 100$ where $\delta_{\max}$ is the maximum angle separation of any two generators at the same time in the post-fault response, and $-100 < \xi < 100$.

To relax the angle-based stability margin to improve the system's transient security after fault, we implement our hierarchical control framework, in which the outputs of fast-acting energy storage are controlled to compensate for

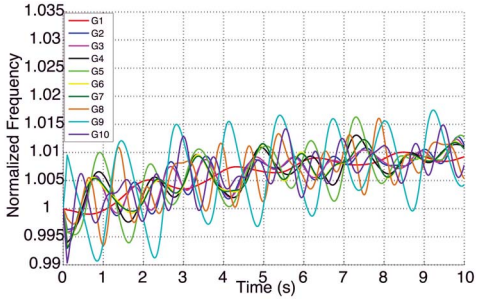

Fig. 9. Normalized rotor frequencies without cyber control for Case Study II.

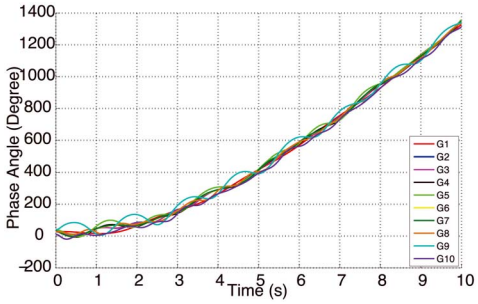

Fig. 10. Phase angles without cyber control for Case Study II.

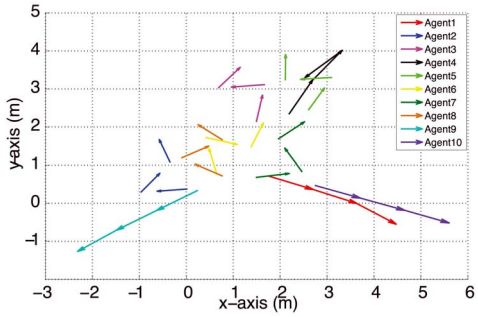

Fig. 11. Trajectories of the boids for Case Study II.

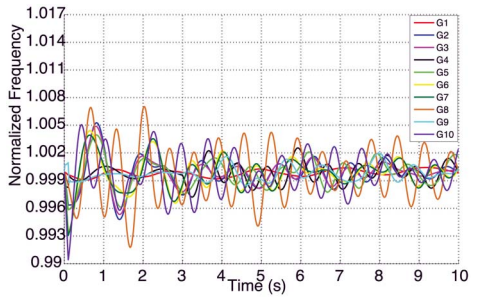

Fig. 12. Normalized rotor frequencies with hierarchical framework.

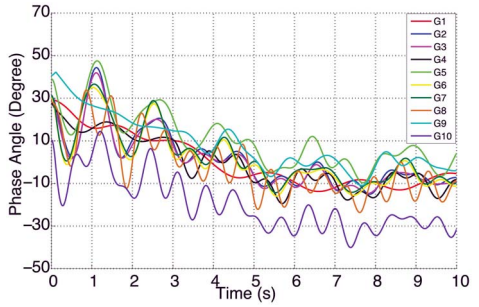

Fig. 13. Phase angles with hierarchical framework.

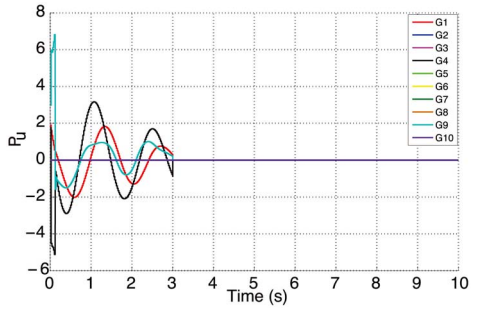

Fig. 14. Power transfer P_u.

demand power's fluctuations caused by the 3-phase short circuit fault.

Our timely dynamic agent coherency identification scheme is implemented immediately after Line $17-27$ is removed at time $t = 0.1$ s. The corresponding boid trajectories introduced by the flocking analogy used in our agent coherency identification scheme is presented in Fig. 11 for a very brief observation period of $t = 0.05$ s. From Fig. 11, we determine that our two-tier hierarchical framework consists of the clusters $\{Agent_1, Agent_{10}\}$, $\{Agent_2, \ldots, Agent_8\}$, and $\{Agent_9\}$, and the lead agents for these three clusters are *Agent* 1, *Agent* 4 and *Agent* 9. After determining the hierarchical framework, our proposed two-tier hierarchical cyber-physical control framework is implemented during time $t = 0.15$ s to 3 s, which is critical maintenance duration. Figs. 12 and 13 evaluate the performance of normalized rotor frequencies and phase angles by using our proposed hierarchical control framework and Fig. 14 shows the power transfer from the fast-acting energy storage to each generator bus. We achieve the angle-based stability margin $\xi_2 = 70.7$, which validates our framework is efficient in improving the transient security of the power system after severe fault.

B. Environment With Practical Constraints of Energy Storage

We evaluate the performance of our hierarchical framework by considering the practical constraints of fast-acting energy storage on power output P_u. We assume the energy storage associated with each Agent i has two constraints: 1) the power output $|P_{u,i}| \leq \rho_1$ p.u. and 2) the rate of the power change $|\Delta P_{u,i}| \leq \rho_2$ p.u./Δt, where $\Delta t = 20$ ms denotes the time step for calculating the control signal for $P_{u,i}$. In the simulation, we consider the same two cases in previous section. Fig. 27 evaluates, given different values of ρ_1, the minimum value of ρ_2 required for maintaining transient stability by using hierarchical and nonhierarchical frameworks in Case I. Fig. 27 also evaluates the minimum value of ρ_2 required for improving ξ equivalent to ensuring $\xi > 57.1$ versus different values of ρ_1 by using hierarchical and nonhierarchical frameworks in Case II. From Fig. 27, it is clear that in Case I, compared to the nonhierarchical framework, the hierarchical framework requires higher but comparable physical requirement for energy storage when $\rho_1 \leq 8$. Fig. 27 also indicates that in Case II, the hierarchical and nonhierarchical framework desire the same physical requirement for energy storage.

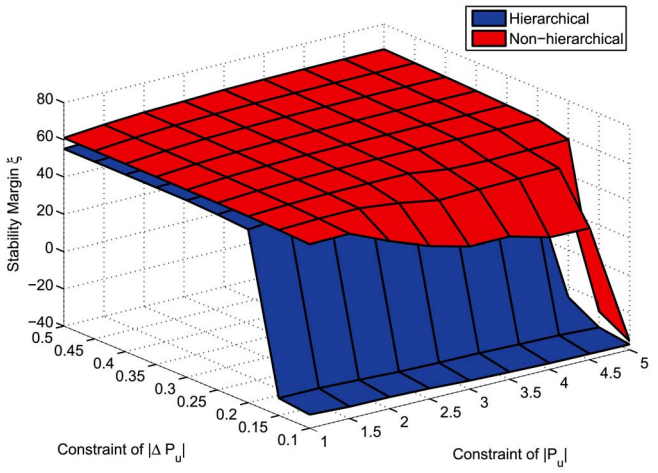

Fig. 15. Stability margin achieved under the practical constraints in Case Study I.

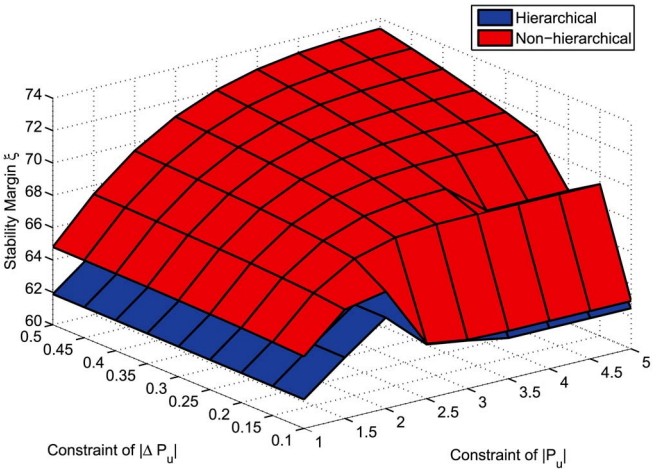

Fig. 16. Stability margin achieved under the practical constraints in Case Study II.

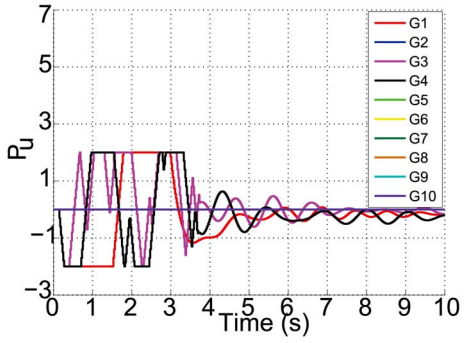

Fig. 17. Power transfer P_u by fast acting energy storage at generator buses.

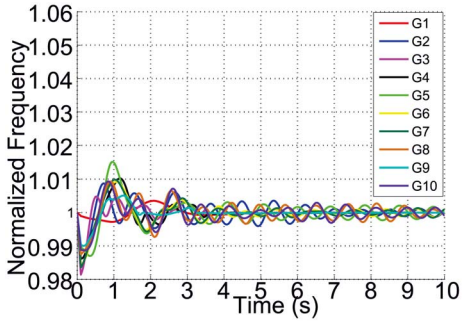

Fig. 18. Normalized rotor frequencies versus time.

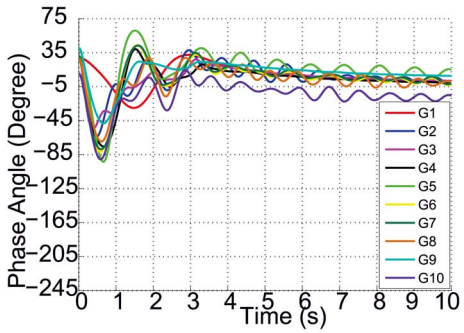

Fig. 19. Phase angles versus time.

In order to analyze the performance of our proposed control framework under the two constraints in more detail, Figs. 15 and 16 evaluate the power angle-based margin ξ achieved by implementing our control framework when $\rho_1 \in [1, 5]$ and $\rho_2 \in [0.1, 0.5]$. From Fig. 15, it is clear that in Case I the proposed hierarchical framework is able to maintain transient stability when $\rho_1 \leq 4.5$ and $\rho_2 \geq 0.2$, or $\rho_1 = 5$ and $\rho_2 \geq 0.2$. From Fig. 16, it is clear that in Case II the proposed hierarchical framework is able to improve the stability margin when $\rho_1 \leq 5$ and $\rho_2 \geq 0.1$. Based on the above observation, we can get that the constraints of the power output and the rate of the power output jointly impact on the performance of the proposed control framework. Furthermore, in both cases, better stability margin can be achieved by implementing the nonhierarchical control framework, but the performance of the hierarchical control framework is comparable with that of the nonhierarchical framework. Therefore, the conclusions obtained from Figs. 15 and 16 are consistent with the conclusion got from Fig. 27. We believe it is reasonable that under the practical physical constraints the nonhierarchical control framework achieves a slightly better results than the hierarchical framework. This is because that in the nonhierarchical framework, more fast-acting energy storage systems (ESSs) are activated which mitigates the impact of the constraints associated with each ESS. Figs. 17–19 show the control signal P_u, the generators' normalized rotor frequency and phase angle by implementing our proposed hierarchical control framework under the constraints $\rho_1 = 2$ p.u. and $\rho_2 = 0.3$ p.u./Δt in Case I. From the simulation results, it is clear that our proposed framework is able to efficiently to maintain transient stability under the practical physical constraints of the fast-acting ESSs.

C. Environment With Communication Delay

We evaluate the performance of our hierarchical framework by studying unexpected communication delay of the PMU data associated with the "lead" agents. As stated in [16]–[18] smart grid communication delay is a significant problem and is typically a result of high network congestion or cyber attack

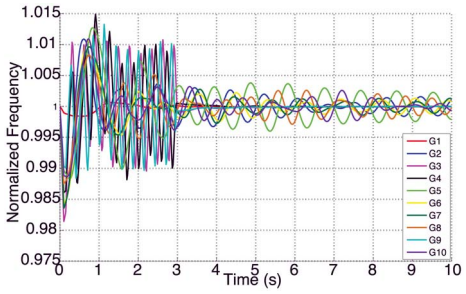

Fig. 20. Normalized rotor frequencies with hierarchical control for fixed communication delay.

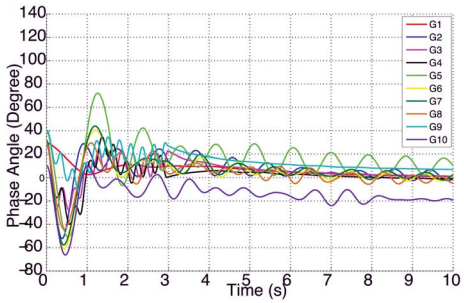

Fig. 21. Phase angles with hierarchical control for fixed communication delay.

such as Denial-of-Service (DoS). Although many attacks often go unreported, recently eurativ.com (10 Dec. 2012), published that a German renewable power grid was hit by a serious communication delay caused by DoS attack [19]. Hence, various researches have been focused on the study of communication delay impacts caused by network congestion or DoS attack on the power grid [20]–[22].

We investigate both fixed and random communication delay for the cases addressed in the previous section. In each case, we consider the situation of unexpected communication delay for $t = 0.2$ s to $t = 3$ s during transient stability maintenance. We assume the phasor data concentrator (PDC) of each cluster employs the following rules to account for delay.

1) The PMU data received by the PDC of each cluster are buffered to guarantee synchronization of the PMU data used in local controller.
2) Until updated again, the control signal P_u is kept the same as the last updated value.
3) If all the PMU data with time stamp $t = k$ are received while the data with time stamp $t = k - 1$ are still buffered, the previous data are dropped and P_u is calculated based on the PMU data with time stamp $t = k$.

1) Fault on Line 14 − 15: We first consider the situation of fixed communication delay. The associated normalized frequencies and phase angles are shown in Figs. 20 and 21. Compared to the performance without delay shown in Fig. 5, the generator frequencies and phase angles both vibrate with higher frequency before $t = 3$ s. This is to be expected as the control is computed based on delayed (or historical) system information that clearly reduces accuracy and timeliness of the commands. Thus, to compensate, the control $\mathbf{u}_l$ must be adjusted with much higher frequency in order to ensure transient stability. The corresponding higher frequency agility of the ESSs' outputs cause frequency vibration of the generator frequencies and phase angles. The hierarchical control, however, still maintains transient stability of the system demonstrating a degree of resilience of our hierarchical framework to communication delay.

We also investigate the situation of random communication delay where the random delay τ is modeled using packet service time statistics in a $M/M/1$ queueing system and defined as follows [23]: $p(\tau) = (1/\kappa)e^{-(\tau/\kappa)}$, where κ denotes the average service time, which is equivalent to average communication delay in our framework.

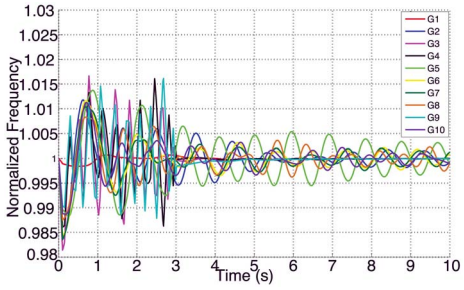

Fig. 22. Normalized rotor frequencies with hierarchical control for random communication delay.

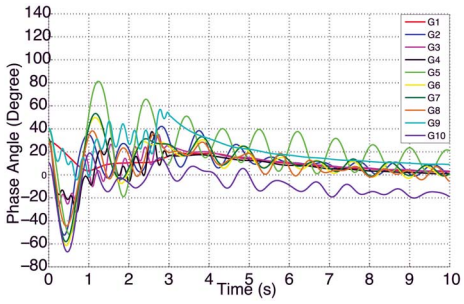

Fig. 23. Phase angles with hierarchical control for random communication delay.

Framework	With fixed delay	With random delay
Nonhierarchical	Transient stability is maintained when $\tau \leq 130$ ms	Success rate is above 95 % when $\kappa \leq 60$ ms
Hierarchical	Transient stability is maintained when $\tau \leq 130$ ms	Success rate is above 95 % when $\kappa \leq 110$ ms

Fig. 24. Comparison between performances of nonhierarchical and hierarchical frameworks.

Assigning the average communication delay to be 60 ms, the system performance is presented in Figs. 22 and 23 from which it is clear that in comparison to the fixed delay case, random delay having the same average value causes vibration with larger amplitude. The system is, however, also resilient to this form of delay.

Fig. 24 summarizes and compares the delay performance of both the nonhierarchical and hierarchical cases. It is clear that both frameworks exhibit the same degree of resilience for maintaining transient stability to fixed communication delay and that the hierarchical framework has greater

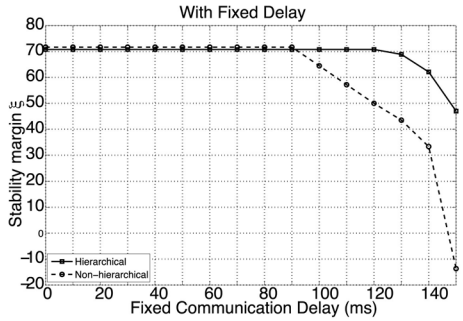

Fig. 25. Stability margin ξ for fixed communication delay.

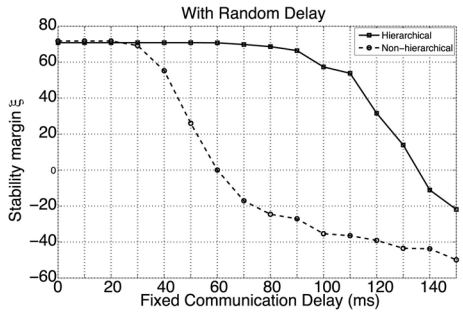

Fig. 26. Stability margin ξ for random communication delay.

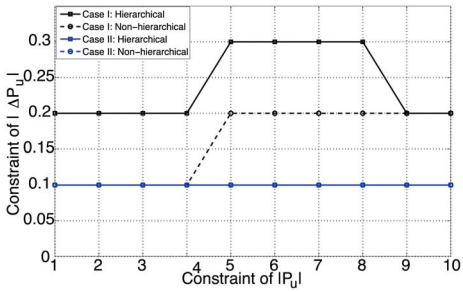

Fig. 27. Performance evaluation of Cases I and II by considering physical constraints of fast-acting energy storage.

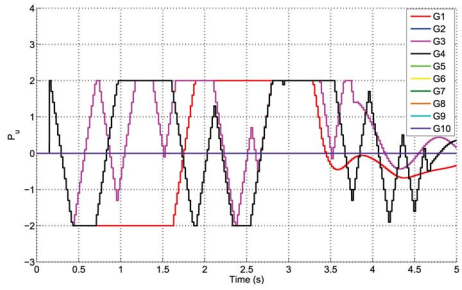

Fig. 28. Power transfer P_u by fast-acting ESS at generator buses when $P^0_{u,i} = 2$ p.u.

resilience to random communication delay. This is reasonable as the nonhierarchical framework requires greater data acquisition and consumption than the hierarchical and that this greater information dependence makes it more susceptible to delays.

For the case of fixed communication delay the difference in resilience for the hierarchical and nonhierarchical cases is negligible. We surmise that this is because in the fixed delay case, the distributed controls that actuate the lead generators are synchronized with respect to each other although they are slightly delayed with respect to the secondary generators. Thus, the controls are still cooperative in nature relative to one another and their strong physical couplings to the secondary generators enable those secondary generators to follow suit (much like if they had their own delayed controls actuating change) enabling transient stabilization with a similar degree of delay. Therefore, we deduce that the hierarchical framework exhibiting reduced overhead also shows advantages in terms of resilience to communication delay especially in case of random delay.

2) Fault on Line 17 − 27: The performance of hierarchical and nonhierarchical frameworks in improving the power angle-based stability margin ξ are evaluated in Figs. 25 and 26. Fig. 25 considers the situation of fixed communication delay and plots the stability margin ξ versus the value of communication delay. Fig. 26 considers the situation of random communication delay and presents the stability margin ξ versus the value of average communication delay. From Fig. 25, it is clear that when the fixed communication delay $\tau \leq 90$ ms, employing the nonhierarchical framework achieves a slightly better stability margin than employing the hierarchical framework. However, when $\tau > 90$ ms, the performance of the nonhierarchical framework becomes dramatically worse compared to the performance of hierarchical framework.

As stated in Section V-A2, the stability margin of the system is $\xi = 57.1$ when no control is applied. From Fig. 25, we observe that to achieve an improvement in stability margin, the fixed communication delay should be $\tau \leq 110$ ms for nonhierarchical control and $\tau \leq 140$ ms using the hierarchical framework. From Fig. 26, we also observe that for random communication delay $\kappa \geq 20$ ms, the performance of the nonhierarchical framework becomes dramatically worse compared to the performance for the hierarchical framework. To improve the stability margin over the no control case, the average communication delay should be $\kappa \leq 40$ ms and $\tau \leq 100$ ms for the nonhierarchical and hierarchical cases, respectively thus demonstrating the greater negative impact of random delay on the performance of both hierarchical and nonhierarchical frameworks.

D. Performance Under Varying Initial Conditions

We evaluate the transient performance of our hierarchical framework in Case I as a function of the initial condition of u_i. We initialize the control signal $u_i = P_{u,i}$ for each Lead Agent i with different values $P^0_{u,i} \in [-\rho_1, \rho_1]$ p.u., where ρ_1 p.u. is the maximum power output constraint of each ESS. For this paper, we consider the physical constraints of the fast-acting ESSs to be $\rho_1 = 2$ p.u. and $\rho_2 = 0.3$ p.u./Δt.

We first consider the situation in which the cyber-physical controllers are activated with $P^0_{u,i} = 2$ p.u. The ESS power output $P_{u,i}$ is shown in Fig. 28. From Fig. 28, it is clear that the power transfers between the lead agents and their associated ESSs are initialized to be 2 p.u. at time $t = 0.15$ s when the cyber-physical controllers are activated, and are updated

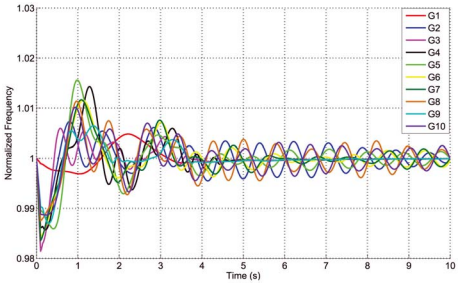

Fig. 29. Normalized rotor frequencies versus time when $P^0_{u,i} = 2$ p.u.

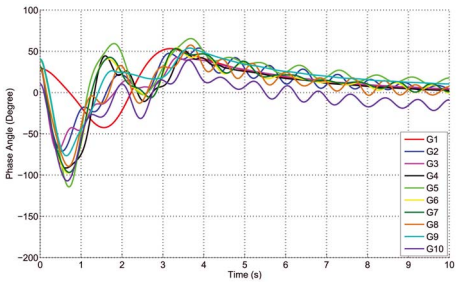

Fig. 30. Phase angles versus time when $P^0_{u,i} = 2$ p.u.

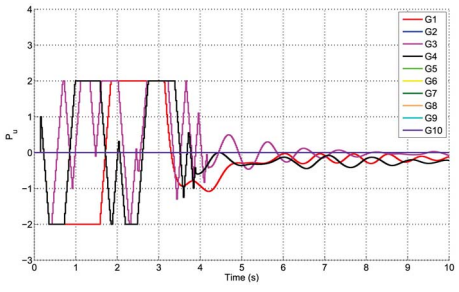

Fig. 31. Power transfer P_u by fast-acting ESS at generator buses when $P^0_{u,i} = 1$ p.u.

via (23) from $t = 0.17$ s onward. The associated normalized frequencies and phase angles are shown in Figs. 29 and 30. From Figs. 29 and 30, we observe that our proposed hierarchical framework is able to maintain the transient stability when the control signal is initialized to $u_i = 2$ p.u. Compared to the performance with initialization $u_i = 0$ p.u. shown in Figs. 18 and 19, we observe that although the initial transient performances are different, the power system is destabilized each time.

Similarly, Figs. 31–33 present the performance of our proposed hierarchical framework with the initial value $u_i = 1$ p.u. From Figs. 31–33, we can also deduce that our hierarchical framework is able to stabilize the power system after a severe physical disturbance regardless of the initial value of u_i. This conclusion is compatible with the proof in the Appendix which shows that the ability of our hierarchical framework to maintain the transient stability of the power system is determined by the design of $\dot{u}_i$ and not its initial condition.

Therefore, without any additional constraint, it is reasonable to set the initial value of the control signal by using two strategies: 1) initializing u_i as 0 p.u. and 2) initializing

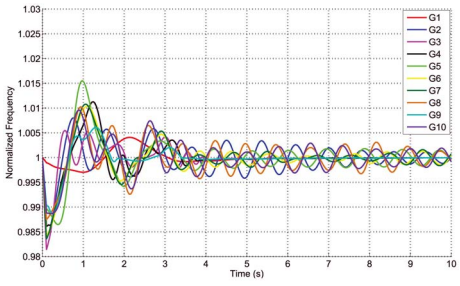

Fig. 32. Normalized rotor frequencies versus time when $P^0_{u,i} = 1$ p.u.

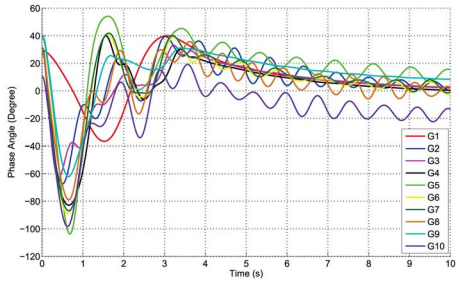

Fig. 33. Phase angles versus time when $P^0_{u,i} = 1$ p.u.

u_i as a uniform random variable with the range of $[-\rho_1, \rho_1]$. We compare these two strategies by evaluating the transient performance of the power system in terms of power angle-based stability margin ξ. $\xi = 58.66$ is achieved by using the first strategy and $\bar{\xi} = 58.03$ is achieved by using the second strategy, where $\bar{\xi}$ is the average of ξ obtained from 100 independent trials. Thus, we conclude that these two strategies achieve comparable transient performance and consider the first strategy in our approach.

VI. Conclusion

In this paper, we have demonstrated one approach to harness physical couplings within a power grid system to enable the selective use of cyber data acquisition and distributed control using a flocking-based paradigm. Within the two-tier multiagent framework, distributed cyber-control is applied at lead generators to achieve first-tier transient stability. Physical coherence is exploited so that secondary agents coupled to lead agents also achieve second-tier synchronization. Analysis and empirical results support our approach. Although this paper provides communication delay performance results applicable to some forms of DoS, the emphasis of the paper is on the introduction of a modeling and distributed control framework and not on cyber security. The interested reader is referred to [24] for a more comprehensive understanding of the effects of more general cyber attacks such as false data injection. Ongoing research focuses on theoretically analyzing the impact of the initial value of the control signal on the transient performance during stabilization.

Appendix

Proof: We define the following Lyapunov function H:

$$H = \frac{1}{2}\boldsymbol{\omega}_l^T \boldsymbol{\mathcal{M}}_l \boldsymbol{\omega}_l + V(\boldsymbol{\theta}_l) \tag{31}$$

for which $H(\mathbf{0},\mathbf{0})=0$ and $H(\boldsymbol{\theta},\boldsymbol{\omega}_l)>0$ for $\forall(\boldsymbol{\theta},\boldsymbol{\omega}_l)\neq(\mathbf{0},\mathbf{0})$. Calculating the derivative of H along the dynamics derived in (21) we obtain

$$\dot{H}=\boldsymbol{\omega}_l^T\boldsymbol{\mathcal{M}}_l\dot{\boldsymbol{\omega}}_l+\boldsymbol{\omega}_l^T\nabla V(\boldsymbol{\theta}_l)=\boldsymbol{\omega}_l^T\boldsymbol{\mathcal{M}}_l\dot{\boldsymbol{\omega}}_l+\boldsymbol{\omega}_l^T\Phi. \quad (32)$$

Based on (21), we have the following:

$$\Phi=-\boldsymbol{\mathcal{M}}_l\dot{\boldsymbol{\omega}}_l-\widetilde{\mathbf{L}}\boldsymbol{\omega}_l-c_1\boldsymbol{\omega}_l-\widehat{\mathbf{S}}\boldsymbol{\Delta}. \quad (33)$$

By substituting (33) into (32), we have

$$\dot{H}=-\boldsymbol{\omega}_l^T\left(\widetilde{\mathbf{L}}+c_1\mathbf{I}\right)\boldsymbol{\omega}_l-\boldsymbol{\omega}_l^T\widehat{\mathbf{S}}\boldsymbol{\Delta}. \quad (34)$$

Based on our proposed framework, $\widetilde{\mathbf{L}}$ is the effective Laplacian matrix which is PSD and $c_1>0$. Therefore, $\left(\widetilde{\mathbf{L}}+c_1\mathbf{I}\right)$ is a Positive Definite (PD) matrix, and thus $\boldsymbol{\omega}_l^T\left(\widetilde{\mathbf{L}}+c_1\mathbf{I}\right)\boldsymbol{\omega}_l>0$.

Since information on $\boldsymbol{\omega}_l$ and $\widehat{\mathbf{S}}$ is available and $\widetilde{\mathbf{L}}$ and c_1 are designable, using Lyapunov redesign method, we obtain

$$\dot{H}\leq-\lambda_m\|\boldsymbol{\omega}_l\|^2+\rho\|\boldsymbol{\omega}_l\|\|\widehat{\mathbf{S}}\|=-\|\boldsymbol{\omega}_l\|\left(\lambda_m\|\boldsymbol{\omega}_l\|-\rho\|\widehat{\mathbf{S}}\|\right) \quad (35)$$

where λ_m is the smallest eigenvalue of $\left(\widetilde{\mathbf{L}}+c_1\mathbf{I}\right)$.

Since $\widetilde{\mathbf{L}}$ is a Laplacian with minimum eigenvalue 0, $\lambda_m=c_1$. Therefore, $\dot{H}<0$ is guaranteed when the following condition is satisfied:

$$\|\boldsymbol{\omega}_l\|\geq\frac{\rho}{c_1}\|\widehat{\mathbf{S}}\|. \quad (36)$$

The high physical coherency between intracluster agents ensures that ρ is sufficiently small. In practice, the tolerance interval of the normalized relative frequency is $[-0.02, 0.02]$, and thus $\rho<0.02$ Therefore, we can design c_3 to satisfy

$$c_1\geq\frac{\rho\|\widehat{\mathbf{S}}\|}{0.02}. \quad (37)$$

Based on (36) and (37), we deduce that $\dot{H}<0$ if $\|\omega_i\|>0.02$, where $i=1,2,\ldots,C$. Thus, the frequencies of all the lead agents are bounded within the required tolerance interval $[-0.02, 0.02]$. Thus, our proposed distributed control guarantees transient stability given the existence of an accurate and efficient coherent cluster identification algorithm.

REFERENCES

[1] M. Ilić, L. Xie, U. Khan, and J. Moura, "Modeling future cyber-physical energy systems for distributed sensing and control," *IEEE Trans. Syst., Man, Cybern. A, Syst., Humans*, vol. 40, no. 4, pp. 825–838, Jul. 2010.

[2] H. Li and Z. Han, "Synchronization of power networks without and with communication infrastructures," in *Proc. IEEE Conf. Smart Grid Commun.*, Brussels, Belgium, Oct. 2011, pp. 463–468.

[3] J. Wei, D. Kundur, T. Zourntos, and K. Butler-Purry, "A flocking-based dynamical systems paradigm for smart power system analysis," in *Proc. IEEE Power Energy Soc. Gen. Meeting*, San Diego, CA, USA, Jul. 2012.

[4] P. Kundur, *Power System Stability and Control*. New York, NY, USA: McGraw-Hill, 1994.

[5] P. Kundur *et al.*, "Definition and classification of power system stability: IEEE/CIGRE joint task force on stability terms and definitions," *IEEE Trans. Power Syst.*, vol. 19, no. 3, pp. 1387–1401, Aug. 2004.

[6] P. Sauer and M. Pai, *Power System Dynamics and Stability*. Upper Saddle River, NJ, USA: Prentice Hall, 1997.

[7] F. Dörfler and F. Bullo, "Synchronization and transient stability in power networks and non-uniform Kuramoto oscillators," in *Proc. Amer. Control Conf.*, Baltimore, MD, USA, Jun./Jul. 2010, pp. 930–937.

[8] F. Dörfler, M. Chertkov, and F. Bullo, "Synchronization in complex oscillator networks and smart grids," *Proc. Nat. Acad. Sci. USA*, vol. 110, no. 26, pp. 2005–2010, Feb. 2013.

[9] C. Reynolds, "Flocks, herds, and schools: A distributed behavioral model," *Comput. Graph.*, vol. 21, no. 4, pp. 25–34, Jul. 1987.

[10] R. Olfati-Saber, "Flocking for multi-agent dynamic systems: Algorithms and theory," *IEEE Trans. Autom. Control*, vol. 51, no. 3, pp. 401–420, Mar. 2006.

[11] A. R. Bergen and V. Vittal, *Power Systems Analysis*. Upper Saddle River, NJ, USA: Prentice Hall, 1999.

[12] H. Khalil, *Nonlinear Systems*. Upper Saddle River, NJ, USA: Prentice-Hall, 2002.

[13] M. Klein, G. Rogers, and P. Kundur, "A fundamental study of inter-area oscillations in power systems," *IEEE Trans. Power Syst.*, vol. 6, no. 3, pp. 914–921, Aug. 1991.

[14] J. Wei and D. Kundur, "A multi-flock approach to rapid dynamic generator coherency identification," in *Proc. IEEE Power Energy Soc. Gen. Meeting*, Vancouver, BC, Canada, Jul. 2013, pp. 1–5.

[15] T. Athay, R. Podmore, and S. Virmani, "A practical method for the direct analysis of transient stability," *IEEE Trans. Power App. Syst.*, vol. PAS-98, no. 2, pp. 573–587, Mar. 1979.

[16] J. McDonald, *Electric Power Substations Engineering* (Electrical Engineering Handbook), 3rd ed. Boca Raton, FL, USA: CRC Press, 2012.

[17] T. Flick and J. Morehouse, *Securing the Smart Grid: Next Generation Power Grid Security*. Boston, MA, USA: Syngress, 2011.

[18] N. R. C. of the National Academies, *Terrorism and the Electric Power Delivery System*. Washington, DC, USA: National Academies Press, 2012.

[19] (2012, Dec. 10). *European Renewable Power Grid Rocked by Cyber-Attack* [Online]. Available: http://www.euractiv.com

[20] E. Hossain, Z. Han, and H. Poor, *Smart Grid Communications and Networking*. Cambridge, U.K.: Cambridge Univ. Press, 2012.

[21] D. Jin, D. M. Nicol, and G. Yan, "An event buffer flooding attack in DNP3 controlled SCADA systems," in *Proc. 2011 Winter Simul. Conf.*, Phoenix, AZ, USA, pp. 2614–2626.

[22] Z. Lu, X. Lu, W. Wang, and C. Wang, "Review and evaluation of security threats on the communication networks in the smart grid," in *Proc. IEEE Military Commun. Conf.*, San Jose, CA, USA, Oct. 2010, pp. 1830–1835.

[23] S. Ross, *Introduction to Probability Models*. Amsterdam, The Netherlands: Academic Press, 2009.

[24] J. Wei, D. Kundur, T. Zourntos, and K. Butler-Purry, "Probing the telltale physics: Towards a cyber-pysical protocol to mitigate information corruption in smart grid systems," in *Proc. IEEE Int. Conf. Smart Grid Commun.*, Tainan, Taiwan, Nov. 2012, pp. 372–377.

Jin Wei (S'09)received the B.E. degree in electronic information engineering from the Beijing University of Aeronautics and Astronautics, Beijing, China, in 2004; the M.S. degree in electrical engineering from the University of Hawaii at Manoa, Honolulu, HI, USA, in 2008; and the Ph.D. degree in electrical and computer engineering from the University of Toronto, Toronto, ON, Canada, in 2014.

She is an Assistant Professor in Electrical and Computer Engineering with the University of Akron, Akron, OH, USA. She was a Post-Doctoral Fellow with the National Renewable Energy Laboratory (NREL), Golden, CO, USA, in 2014. Her current research interests include the cyber-physical energy system, cyber-physical systems security, renewable energy integration, stochastic modeling and optimization of large-scale systems, and cognitive wired/wireless communication networks.

Dr. Wei has been the recipient of travel grants and is an IEEE Canadian Conference on Electrical and Computer Engineering'12 Best Student Paper Finalist.

Deepa Kundur (SM'03) received the B.A.Sc., M.A.Sc., and Ph.D. degrees in electrical and computer engineering from the University of Toronto, Toronto, ON, Canada, in 1993, 1995, and 1999, respectively.

She is a Professor of Electrical and Computer Engineering at the University of Toronto. Her current research interests include cyber security of the electric smart grid, cyber-physical system theory, security and privacy of sensor networks, and multimedia security and forensics.

Dr. Kundur has served on the North American Reliability Corporation Smart Grid Task Force, has been on several editorial boards, and currently serves as an Associate Editor of the IEEE TRANSACTIONS ON INFORMATION FORENSICS AND SECURITY. Her research has received best paper recognitions at the 2008 IEEE International Conference on Computer Communications Workshop on Mission Critical Networks, the 2011 Cyber Security and Information Intelligence Research Workshop, the 2012 IEEE Canadian Conference on Electrical and Computer Engineering, and the 2013 IEEE Power and Energy Society General Meeting.

Takis Zourntos (SM'09) received the B.A.Sc. (Hons.) degree in engineering science, and the M.A.Sc. and Ph.D. degrees in electrical and computer engineering from the University of Toronto, Toronto, ON, USA, in 1993, 1996, and 2003, respectively. He is currently pursuing the Master's degree in fine arts at the Ontario College of Art and Design, University in Toronto, specializing in interdisciplinary art, media, and design.

From 1998 to 2001, he was a Co-Founder of Protolinx Corporation, Etobicoke, Toronto, ON, Canada, a start-up developing high-speed wireless communications technology. From 2003 to 2013, he was affiliated with Texas A&M University, College Station, TX, USA, most recently conducting research in robotics and power systems as a Research Faculty Member in Computer Science. He has 47 publications to his credit.

Dr. Zourntos has received the 2003 IEEE Best Professor Teaching Award from his students at Texas A&M University. Along with his collaborators, he received a Best Paper Award from the 2011 Cyber Security and Information Intelligence Research Workshop for a novel power system switching attack paradigm, the 2009 Best of What's New Award from *Popular Science* magazine for the Survivor Buddy Robot, and received coverage on wired.com for a robotically-enhanced theater.

Karen L. Butler-Purry (SM'01) received the B.S. degree (*summa cum laude*) in electrical engineering from Southern University, Baton Rouge, LA, USA, in 1985; the M.S. degree in electrical engineering from the University of Texas at Austin, Austin, TX, USA, in 1987; and the Ph.D. degree in electrical engineering from Howard University, Washington, DC, USA, in 1994.

She joined Texas A&M University, College Station, TX, in 1994, where she currently serves as an Associate Provost for Graduate Studies and as a Professor with the Department of Electrical and Computer Engineering. Her current research interests include distribution automation, cyber physical systems protection, and intelligent systems for power quality, equipment deterioration, and fault diagnosis.